

Detailed Flow Field around a Leading-Edge Slat at Low Reynolds Numbers

Sanehiro MAKIYA*, Ayumu INASAWA* and Masahito ASAI*

*Dept. of Aerospace Eng., Tokyo Metropolitan University,

Abstract

Flows around a leading-edge slat are investigated experimentally at Reynolds numbers $Re \leq 5.2 \times 10^5$. When the slat operates to suppress the leading-edge stall, a periodic vortex shedding occurs due to the instability of laminar wake of the slat at Reynolds numbers less than 2.1×10^5 . The Reynolds number variation of the shedding frequency is not unlike that of the circular-cylinder wake at low Reynolds numbers. For $Re \geq 2.3 \times 10^5$, prominent spectral peaks appear both in the velocity fluctuations and sound-pressure and the frequency of such distinguished noise is found to be proportional to $U_\infty^{0.84}$ as reported in the experiment on the sound generation in a single-element airfoil at small angles of attack, suggesting a possibility of feedback loop between the shear layer instability immediately upstream the slat trailing-edge and the generated sound.

Key Words: Leading-edge slat, Instability, Vortex shedding, Aeroacoustics

1. Introduction

The leading-edge slat is a high-lift device widely used together with the rear flap to suppress the stall of aircraft at high angles of attack. Numerous experimental and computational studies have been conducted on the aerodynamic characteristics of multi-element airfoil⁽¹⁻³⁾. On the contrary to the high-lift achievement, the leading-edge slat gives rise to additional airframe noise, which may be a serious problem in advanced aircraft design. Indeed, slat-generated noise is known to be a significant contributor to the airframe noise during the landing phase, and its reduction is one of the most important and challenging technologies for the aircraft development.

Recent computational studies⁽⁴⁻⁸⁾ on the aeroacoustics of multi-element wing indicate that slat noise consists of broadband low- and mid-frequency components probably originating in the slat cove and narrowband higher-frequency components generated at and around the slat trailing-edge. However, few experiments have been reported on the flow field and the related aeroacoustics of the slat. In the present experimental study, in order to better understand the flow phenomena and noise generation, the flow field around the slat is investigated in detail.

2. Experimental setup and procedure

The experiment is conducted in an open-jet type wind tunnel with exit cross-section of 600 mm (height) \times 300 mm (span). Experimental setup is illustrated in Fig. 1. Two Plexiglas sidewalls are installed in the test section to keep two-dimensionality

of the main stream though upper and lower areas are opened. A three-element wing model is set between the sidewalls. The configuration of the wing model is illustrated in Fig. 2. The stowed wing consists of a NACA23012 airfoil section and its chord c is 300 mm. In the present experiment, the wing is kept unflapped and only the slat is displaced along the chord line of the stowed wing section.

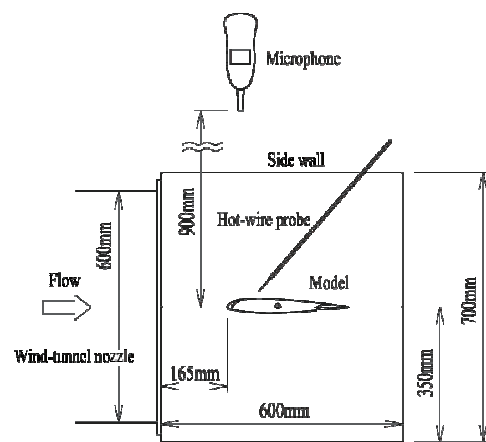


Fig. 1. Experimental setup.

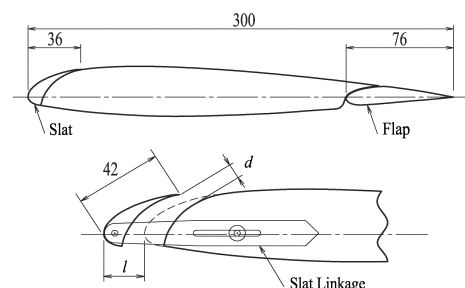


Fig. 2. Configuration of three-element wing model.

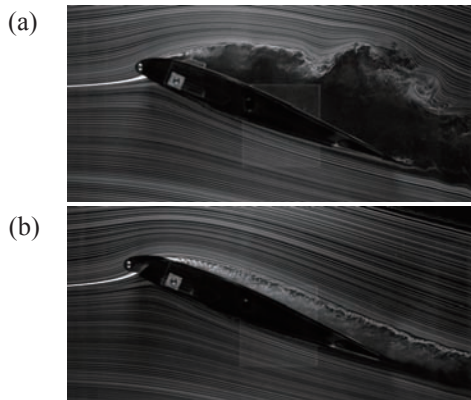


Fig. 3. Flow past NACA23012 airfoil at $\alpha = 20^\circ$, $Re = 8.2 \times 10^4$. (a) No slat gap, (b) slat gap $d = 3.1$ mm ($l = 10$ mm).

The velocity measurements are made using a constant-temperature hot-wire anemometer. To measure aerodynamic noise, a high-precision microphone (LION NL-22) is set 900 mm above the slat trailing edge. Flow visualization is done by means of smoke-wire technique. Two smoke-wires are stretched in the vertical and spanwise directions and still camera shots are taken with stroboscopic light. Movies of smoke-wire visualization are also taken by using a high-speed digital video camera.

The free-stream velocity U_∞ ranges from 2 m/s to 25 m/s and the corresponding Reynolds number based on the stowed-geometry wing chord is $Re = 4.2 \times 10^4$ to 5.2×10^5 .

3. Results and discussion

In the case of stowed configuration, the airfoil stall occurs at angles of attack α higher than 18° , as shown in Fig. 3(a) which visualizes the flow at $\alpha = 20^\circ$ at $Re = 8.2 \times 10^4$. When the slat gap is adjusted properly, the leading-edge stall is completely suppressed at the same angle of attack, as shown in Fig. 3(b). Fig. 4(a) shows a close-up view of the smoke visualization picture of the flow around the slat. When the leading-edge stall is suppressed, we can see a quite periodic vortex shedding from the trailing edge of the slat. In the figure, a laminar separation bubble in the cove region is also seen clearly. Owing to the low Reynolds number $Re = 8.2 \times 10^4$, the separation bubble in the cove remains laminar without noticeable development of Kelvin-Helmholtz instability. Fig. 4(b) displays a top view of visualization, showing that the shedded vortices are almost two-dimensional.

Figs. 5(a) and (b) display the y -distributions of time-mean velocity U and r. m. s. value of velocity

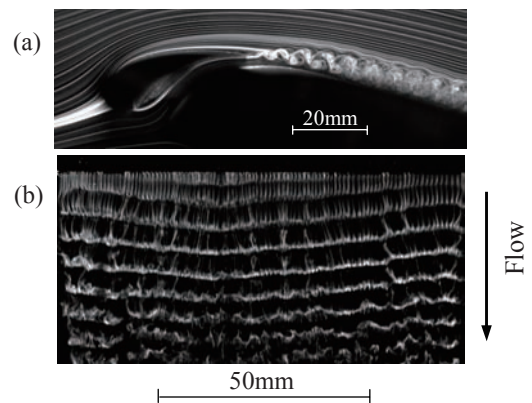


Fig. 4. Flow visualization of the slat wake ($d=3.1$ mm) at $\alpha = 20^\circ$, $Re = 8.2 \times 10^4$. (a) Side view, (b) top view.

fluctuation u' in the near-wake region, 1 mm and 4 mm downstream the slat trailing-edge, respectively. Here, the normal-to-wall coordinate y measures from the surface of the main element. As seen from Fig. 5(a), both the flows passing upper and lower surfaces of the slat accelerate to $1.5U_\infty$. Consequently, the slat wake seems to be that of an airfoil in a uniform flow, though the upper shear layer is thicker than the lower shear layer. A reversed flow region appears between $y = 3.6$ mm and 4.6 mm, as seen from the fact that the velocity decreases to zero at $y = 3.6$ mm and 4.6 mm and increases slightly between these two y -positions: Note that the hot-wire can not sense the flow direction. The velocity distribution with the reversed flow has the nature of absolute instability, which is prerequisite for the onset of global instability, i.e., onset of the periodic wake oscillation⁽⁹⁾. The reversed flow disappears at the location 4 mm downstream the slat trailing-edge as shown in Fig. 5(b). The wake width (defined as the half-value width) is about 1.5 mm so that the streamwise distance of the reversed flow region is not larger than three times the wake width. The present result shows that such streamwise extent of reversed flow region is sufficient for the occurrence of global instability. The peak values of u' in the upper and lower shear layers already exceed $0.15U_\infty$ at this location, which corresponds to the development of wake vortices visualized in Figs. 3 and 4. In Fig. 5(b), we also notice that the two peaks in the u' distribution (at $y = 3.5$ mm and 4.6 mm) are not the same in magnitude, which is due to the difference in the intensity of the velocity gradient (or the shear layer thickness).

Next examined is how the disturbance frequency changes with the free-stream velocity. To avoid

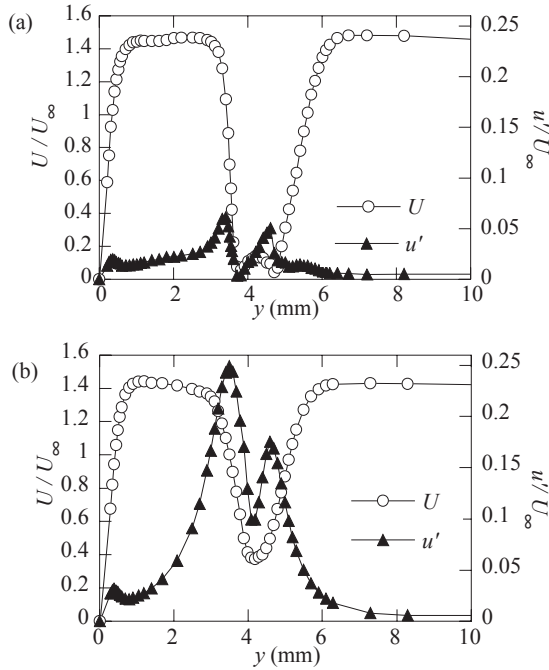


Fig. 5. Mean velocity U and r. m. s. value of velocity fluctuation u' , (a) 1 mm and (b) 4 mm from the slat trailing-edge at $U_\infty = 4$ m/s ($Re = 8.2 \times 10^4$).

possible interferences with the flow, particularly the flow between the slat and the main wing-element, the hot-wire probe is set outside the slat wake (10 mm downstream the slat trailing-edge and $y = 6.4$ mm). Fig. 6 illustrates the relation between the free-stream velocity and the dominant disturbance frequency (its fundamental component). A discontinuity in the dominant frequency occurs between $U_\infty = 10$ m/s ($Re = 2.1 \times 10^5$) and 11 m/s ($Re = 2.3 \times 10^5$). This suggests that the mechanism of vortex generation changes around there ($U_\infty = 10 \sim 11$ m/s). Fig. 7 shows that the Strouhal number based on the thickness of slat trailing-edge t_s ($= 0.5$ mm) St ($= ft_s/U_\infty$) against the trailing-edge-thickness Reynolds number Re_{t_s} ($= U_\infty t_s/\nu$) for $U_\infty \leq 10$ m/s. St increases gradually to approach 0.12 for $Re_{t_s} > 200$. Such a variation in St against Re is quite similar to the case of circular-cylinder wake⁽¹⁰⁾.

Figs. 8(a) and (b) show the power spectrum of velocity fluctuation and the sound pressure level (SPL) distribution (measured by the microphone above the slat trailing-edge), respectively. The measurements are made at $U_\infty = 6$ m/s ($Re = 1.3 \times 10^5$). We can see distinct peaks at $f = 1416$ Hz and at its harmonic frequencies in the power spectrum of the velocity fluctuation (Fig. 8a). This no doubt results

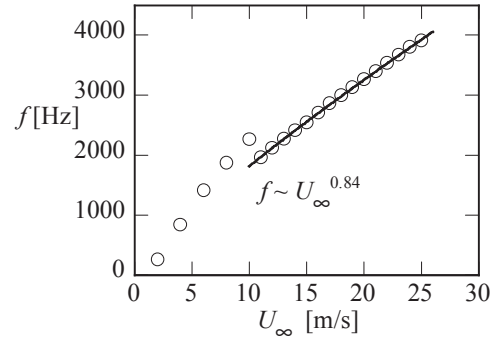


Fig. 6. Noise frequency vs. free-stream velocity.

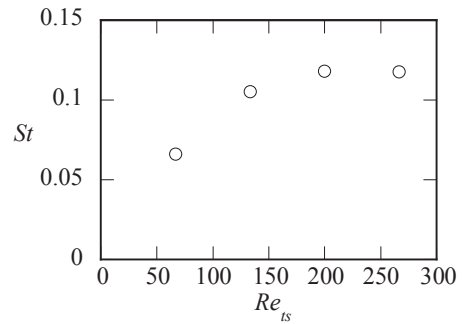


Fig. 7. Strouhal number vs. Reynolds number for $U_\infty \leq 10$ m/s ($Re \leq 2.1 \times 10^5$). t_s is the thickness of the slat trailing-edge.

from the absolute instability of slat wake as mentioned above. On the other hand, we see no distinct peak for the SPL spectrum (Fig. 8b). Thus, sound generation is extremely weak at this low Reynolds number even though the strong periodic vortex shedding already occurs.

Figs. 9(a) and (b) show the similar spectra measured at higher free-stream velocity $U_\infty = 19$ m/s ($Re = 4.0 \times 10^5$). Prominent peaks are observed both in the velocity spectrum and the SPL distribution at $f = 3141$ Hz. Such sharp peaks always appear for $U_\infty \geq 11$ m/s ($Re \geq 2.3 \times 10^5$), and the peak frequency (fundamental component) is found to be proportional to $U_\infty^{0.84}$, as already shown in Fig. 6.

On this concern, it should be referred to the experiments⁽¹¹⁾ on the tonal noise from the NACA0012 airfoil at small angles of attack, where the discrete-tone frequency is proportional to $U_\infty^{0.8}$. In that experiment, the shear layer instability of Kelvin-Helmholtz type was observed on the pressure side of the airfoil immediately upstream the trailing edge, and it was pointed out that the frequency of generated sound was close to that of the most amplified disturbance calculated from the linear instability of

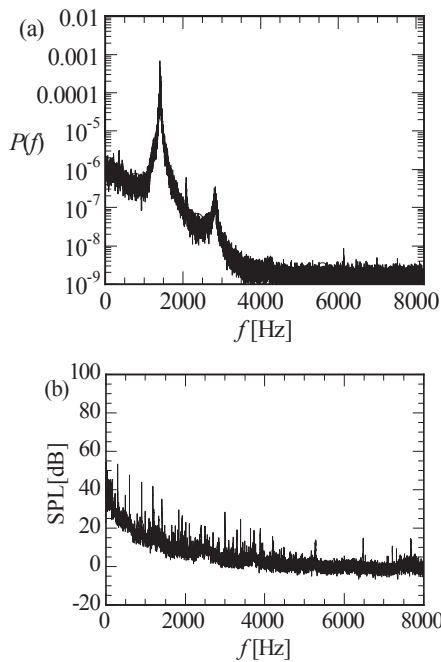


Fig. 8. Power spectrum of the velocity fluctuation in (a) and SPL distribution in (b) at $Re = 1.3 \times 10^5$ ($U_\infty = 6$ m/s).

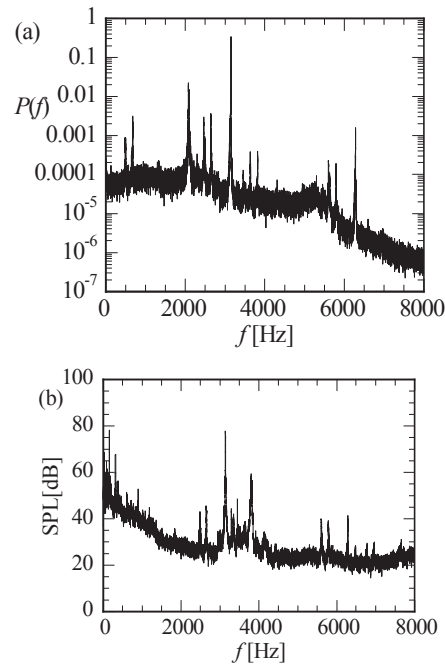


Fig. 9. Power spectrum of the velocity fluctuation in (a) and SPL distribution in (b) at $Re = 4.0 \times 10^5$ ($U_\infty = 19$ m/s).

inflectional velocity profiles near the trailing edge though stability analysis could not explain why the narrow-band peak appears in the spectra. A possible mechanism causing such a discrete peak is the feedback loop through the receptivity process between the shear layer instability and the generated sound though it is not clarified yet.

4. Conclusions

Flows around a leading-edge slat have been investigated experimentally at low Reynolds numbers $Re = 4.2 \times 10^4$ to 5.2×10^5 . The observations have been focused on the flows at a high angle of attack $\alpha = 20^\circ$ where the airfoil undergoes the leading-edge stall for the stowed-geometry case. For $Re \leq 2.1 \times 10^5$, a periodic vortex shedding due to the global instability of the slat wake, which is not unlike in the circular-cylinder wake, occurs, but the associated sound generation is very weak. For $Re \geq 2.3 \times 10^5$, on the other hand, distinguished almost-discrete tone appears and its frequency is proportional to $U_\infty^{0.84}$. Such strong sound generation suggests a possibility of feedback mechanism between the shear layer instability immediately upstream of slat trailing edge and the generated sound, but it still remains open and further investigation is needed.

References

- (1) Nakayama, A. et al.: AIAA J. 28 (1) (1990) pp. 14-21
- (2) Yasuhara, M. et al.: Trans. Jpn. Soc. Aeron. Space Sci., 33 (1991) pp.218-233.
- (3) Maddah, S.R. et al.: Exp. Thermal and Fluid Sci., 25 (2002) pp.651-658.
- (4) Murayama, M. et al.: Trans. Jpn. Soc. Aeron. Space Sci., 49 (2006) pp.40-48.
- (5) Khorrami, M.R. et al.: AIAA J., 38 (11) (2000) pp.2050-2058.
- (6) Khorrami, M.R. et al.: AIAA J., 40 (7) (2002) pp.1284-1291.
- (7) Khorrami, M.R. and Choudhari, M.M.: NASA/TM-2003-212416 (2003).
- (8) Imamura, T. et al.: 12th AIAA/CEAS Aeroacoustics Conference-2006-2668, (2006).
- (9) Huerre P.: Annu. Rev. Fluid Mech., 22 (1990) pp. 473-537.
- (10) Williamson C. H. K.: J. Fluid Mech., 206 (1989) pp.579-627.
- (11) Nash, C. E. et al.: J. Fluid Mech., 382 (1999) pp.27-61.